Granular Matter (2021) 23:6
https://doi.org/10.1007/s10035-020-01071-5

ORIGINAL PAPER

Characterization and modeling of granular jamming: models for mechanical design

Loïc Blanc[1,3] · Bertrand François[2] · Alain Delchambre[3] · Pierre Lambert[1]

Received: 10 April 2020 / Accepted: 26 October 2020

Abstract
The use of granular jamming is proposed for designing structures with tunable rigidity of their tools (with the ability of being flexible devices for shaping and deformation but rigid for shape-locking and force transmission). The granular jamming consists in modifying the apparent rigidity of a structure by controlling the vacuum in a membrane filled with granular material. When the difference of pressure is low, the grains are free to move with respect to each other and the structure is flexible. When the vacuum in the membrane is increased, the grains are blocked and the structure is more rigid. Different mechanical characterizations of the granular jamming have been performed (triaxial compression and tension and cantilever beam bending tests) for different glass bead sizes ranging between 100 µm and 1 mm (used as granular material) at different vacuum levels (between 0 kPa and 90 kPa). The grain size slightly influences the stiffness while the pressure difference is the main parameter to tune the stiffness of the structure. Based on these experiments, analytical models have been developed and validated. The tension characteristics can be directly deduced from the compression behavior and the bending modulus can be obtained by a combination of the tension and compression moduli. The proposed analytical models present the advantage of a simple formulation and are suitable for estimating the performance of other structures based on the granular jamming. The models can estimate and predict satisfactorily the results of granular jamming and can be used for designing mechanical structures based on this mechanism.

Keywords Granular jamming · Triaxial testing · Analytical model · Tunable flexural stiffness · Mechanical design

1 Introduction

Currently, in the medical field, the clinicians are facing a problem about the stiffness of their tools. They need them to be as flexible as possible to travel in the human anatomy without damaging the tissues or causing pain to the patient, but once in position, they need them to be rigid to support additional tools or to perform their tasks (e.g. gripping, suturing, puncturing) [1, 2]. Therefore, the clinicians require tunable stiffness tools. Furthermore, decreased dimensions are preferred to reduce the invasiveness of the medical devices [3]. As reduced dimensions are leading to reduced flexural stiffness EI (given by the product of the elastic modulus E and the second moment of area I), a control on the equivalent elastic modulus could enhance the tools. Such dual requirements on the stiffness of structures are not only present in the medical field, but can be found in, among others, robotics, aerospace engineering or vibration damping [2, 4–6]. For example, robotic arms with controllable stiffness abilities present the advantages of soft robots with numerous degrees of freedom and safe environment interactions in their flexible state, and can develop larger level of forces and accurate motion in their rigid state [7–9].

Many mechanisms have been described in the literature for controlling the stiffness (elastic properties) of structures [4, 10]. The solutions based on the change in mechanical properties of materials by controlling their temperature lead to very large stiffness change, but the actuation time mainly depends on the design and the amount of material to be

✉ Loïc Blanc
loic.blanc@ulb.ac.be

Pierre Lambert
pierre.lambert@ulb.ac.be

[1] TIPs Department, CP165/67, Université Libre de Bruxelles, av.FD Roosevelt 50, 1050 Brussels, Belgium

[2] BATir Department, CP194/2, Université Libre de Bruxelles, av.FD Roosevelt 50, 1050 Brussels, Belgium

[3] BEAMS Department, CP165/56, Université Libre de Bruxelles, av.FD Roosevelt 50, 1050 Brussels, Belgium

Published online: 26 November 2020

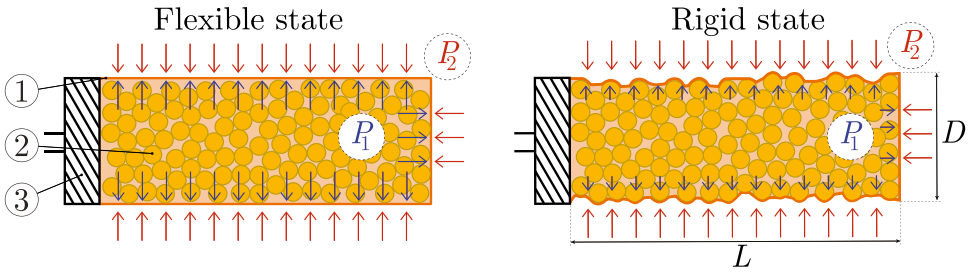

Fig. 1 Granular jamming enables the change in stiffness by modifying the pressure difference $\Delta P = P_2 - P_1$, with P_2 the surrounding pressure and P_1 the pressure in the sample; the sample is composed of the membrane (1), the granular material (2) and the filter (3), with D the sample diameter and L the sample length

heated (and can be long). Solutions based on the locking of structural elements are promising as the stiffness change is very fast (≤ 0.1 s) and can be effective in the entire structure at the same time [2]. One of these promising solutions is the granular jamming [11]. This mechanism has been used for developing universal grippers, as it can be deformed around the object to grasp and become rigid again for lifting [12–15].

1.1 Working principle

The samples are composed of a flexible and airtight membrane filled with a specific granular material as shown in Fig. 1. The stiffness of the sample is related to the pressure difference ΔP across the membrane given by

$$\Delta P = P_2 - P_1, \tag{1}$$

where P_2 is the pressure corresponding to the surrounding environment and P_1 is the pressure measured inside the sample (under the membrane).

When the pressure difference is low ($\Delta P \approx 0 \implies P_1 \approx P_2$, the pressure in the sample is close to the pressure of the surrounding environment), the grains are free to move with respect to each other. In this configuration, the system is in its flexible state, as it presents a lower resistance to deformation (lower stiffness) [12]. When the pressure difference is increased, the system is more rigid as the grains start to be locked to each other. In this new configuration, the sample presents a larger resistance to deformation as the internal reorganization of the grains requires a larger force. The pressure difference is obtained by vacuuming the specimen. Therefore, a filter is required to avoid sucking the granular material in the pump.

The granular jamming principle based on air suction is suitable for medical applications as in case of failure of the vacuum source, the system will remain in its flexible state (as the pressure difference ΔP is low). It is therefore possible to easily remove the device in case of problem during the intervention. The time required to switch from one state to another will depend on the size of the sample and the flow rate of the vacuum pump, but for small size samples, the duration is negligible and an activation time of the order of 0.1 s is easily reached.

1.2 Goal of the research

The main goal of this research is to provide a deep characterization of the granular jamming and an analytical model for evaluating and estimating the performances of the stiffness change of this mechanism. In the literature, the granular jamming is mainly characterized in bending (cantilever beam bending) [7, 16], but mostly in terms of forces and deflections [17–19]. A stress-strain approach is followed in this work for more general interpretation [20]. Furthermore, compression and tension tests are proposed to characterize and compare the performance of the granular jamming under different loading conditions and to understand and model the behavior in bending corresponding to a loading closer to numerous mechanical applications. The models proposed in this work are not targeting specific applications, but are intended to better estimate the performance of the granular jamming for general mechanical structures. Mechanical characterization of granular materials is usually done in

Table 1 The glass beads from *Sigmund Lindner GmbH* are divided in five classes with respect to their range of diameters

Class	Diameters range	Mean diameter	Roundness[a]
A	0.10–0.20 mm	$\bar{d} = 0.17$mm	≥ 0.89
B	0.20–0.30 mm	$\bar{d} = 0.25$mm	≥ 0.89
C	0.30–0.40 mm	$\bar{d} = 0.34$mm	≥ 0.89
D	0.50–0.75 mm	$\bar{d} = 0.68$mm	≥ 0.95
E	0.75–1.00 mm	$\bar{d} = 0.94$mm	≥ 0.95

[a] The roundness is defined as the ratio of the width (smallest dimension in the cross-section) over the length (largest dimension in the cross-section)

compression [12, 20] while most applications of granular materials in robotic structures rather rely on bending [10]. Therefore, this paper proposes a model which links both loading conditions.

2 Materials

The granular materials used in this work are grinding materials (glass beads) from *Sigmund Lindner GmbH*. These beads are polydisperse, polished and made of soda lime glass with a specific weight of 2.5 kgL^{-1}. The elastic modulus of these glass beads is $E_g = 63$ GPa. Five different sets of glass beads with submillimeter diameters are studied. The influence of other granular material properties is proposed in [20]. Their geometrical characteristics are given in Table 1.

In this work, a vacuum pump *VP4300* from *Easy Composites Ltd* is used. This pump has an exhaust flow of 430 L min^{-1} making the state transition from flexible to rigid very fast for small samples. The lowest pressure achievable by the pump is 3.25 Pa (99.995% of the absolute vacuum). An *IRV20* vacuum regulator valve from *SMC Pneumatics* is used to set the desired vacuum level (between 0 kPa and 90 kPa). The filter is made of cotton wool ensuring the air to pass through but blocking the particles. The advantage of this filter is that it can be adjusted to any shape and size and even placed in very small samples. If the filters are too thick or particles are blocking the airflow, the vacuum cannot progress through the sample and the change in stiffness will not be properly observed.

3 Mechanical characterization

The granular jamming solution can be characterized by different mechanical testing methods. As a dry granular material cannot withstand large forces or maintain a given shape

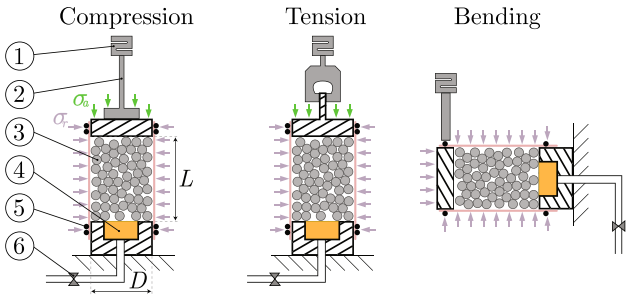

Fig. 2 Triaxial set-ups with the load cell (1), mechanical connection between loading frame and specimen (2), the triaxial test specimen (3), the cotton filter (4), sealing O-rings (5) and the vacuum regulator valve (6); D is the sample diameter and L the sample length, while σ_a is the axial stress and σ_r the radial stress

by itself, it has to be placed in a membrane. The samples for the different mechanical tests are cylinders (for axisymmetry and homogeneous distribution of the pressure difference ΔP). The mechanical tests are performed in order to characterize the samples with several granular materials for different pressure differences. First, triaxial compression tests, routinely used in geomechanics (mainly for characterizing soils under a defined confinement [21]), are performed to characterize the granular material in shearing conditions [22]. Usually, the confinement is set by pressurizing the surrounding environment of the sample, but in this study, the sample is vacuumed. Then, tensile tests are performed to characterize the behavior of the samples in traction. Tensile tests are routinely performed by mechanical and material engineers to characterize a material. In this work, triaxial tensile tests are performed as the pressure difference ΔP is acting as a confinement controlling the radial stress (by vacuuming the samples). Finally, bending tests are performed to characterize the material in a configuration and in loading conditions closer to the final application [22] (with vacuumed samples). The different triaxial testing set-ups are

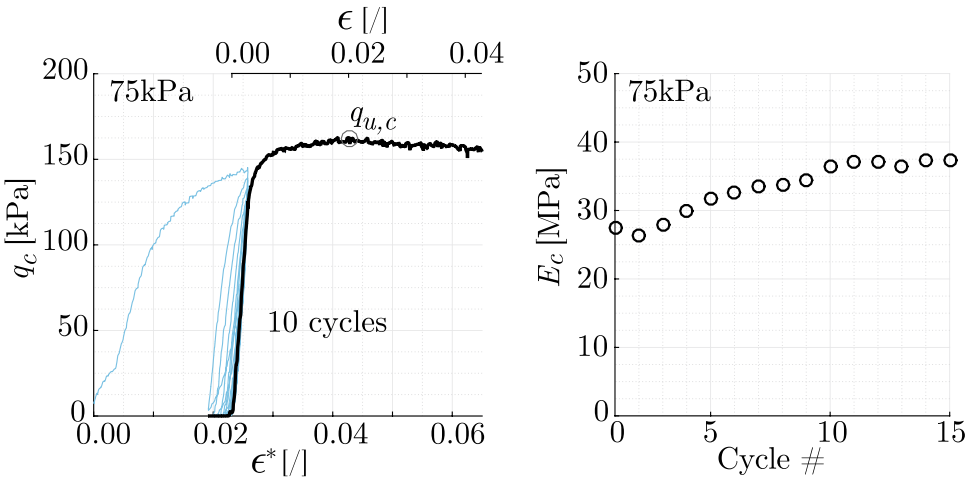

Fig. 3 Deviatoric stress evolution for new equivalent strain with cycling procedure for class E glass beads at $\Delta P = 75$ kPa where the failure is measured at $q_{u,c} \approx 162$ kPa; the new strain ϵ is set to zero after the cycles of loading-unloading while the initial strain ϵ^* actually starts at the beginning of the triaxial compression test; the elastic modulus is stabilizing after 10 cycles

illustrated in Fig. 2. Each test, with each loading condition, is repeated three times for statistical analysis.

A specific cycling procedure is applied to the mechanical tests. The cycling method consists in starting with loading-unloading cycles (ten times) in order to reset the initial conditioning of the granular material in the samples. Such a procedure is illustrated in Fig. 3 and showed encouraging results about the repeatability of triaxial compression testing of dry granular materials [20]. The elastic modulus is stabilizing after ten cycles, therefore for decreased duration of the tests, this number of cycles is used.

In order to remove the influence of the geometry and the dimensions of the samples, a stress-strain analysis is performed instead of the force-displacement characteristic directly obtained from the experiments. In this work, the granular jamming is modeled as an isotropic material. Instead of considering independently the grains forming the structure (as it has been done in a previous work [23]), this solution is studied as an equivalent homogeneous material with similar macroscopic characteristics to apply the classical relationships developed in beam theory.

The sample is cylindrical for axisymmetric analysis, for a proper confinement and for easy loading conditions. The sample has a length L at least (and approximately) twice its diameter D. This ratio is used to ensure a proper observation of shearing [24]. Due to the shape of the sample, the principal stresses can be controlled in the axial and radial directions. The radial stress is directly set by the confinement while the axial stress is initially set by the confinement, but is then increased or decreased and measured during the axial loading or unloading. The sample is therefore placed under a loading frame equipped with an axial force sensor (LS1 universal testing machine from *Lloyd Instrument* in this work). The confinement of the sample has been obtained by connecting the sample to a vacuum pump (through a vacuum regulator valve) to directly set the confining pressure of the sample. The vacuum pump is working during the entire test to ensure a constant difference of pressure.

The radial stress σ_r is set by the confining pressure ΔP, fixed by a pressure controller and defined for each test. The longitudinal or axial stress σ_a is equal to the sum of the confining pressure ΔP and the longitudinal stress applied during the loading or unloading. The deviatoric stress q is defined in Eq. 2 as the difference between the axial stress σ_a and the radial stress σ_r. It corresponds to the stress applied by the loading frame on the sample and is directly calculated from the applied load. The major principal stress σ_1 is the normal stress with the largest value (corresponding to the axial stress in compression and to the radial stress in tension), while the minor principal stress σ_3 is the normal stress with the lowest value (corresponding to the radial stress in compression and to the axial stress in tension).

$$\begin{cases} q_c = \sigma_a - \sigma_r = \sigma_1 - \sigma_3 \\ q_t = \sigma_a - \sigma_r = \sigma_3 - \sigma_1 \end{cases}, \tag{2}$$

with the subscripts c and t for the compression and tension loading respectively.

Another interesting scalar is the mean stress p defined in Eq. 3 as the average of the stresses acting on the sample [25, 26]. At low deviatoric stress q ($\sigma_a \approx \sigma_r, \sigma_1 \approx \sigma_3$), the mean stress p is equivalent to the radial stress (confining pressure) $p \approx \sigma_r = \Delta P$.

$$p = \frac{\sigma_a + 2\sigma_r}{3} \implies \begin{cases} p_c = \frac{\sigma_1 + 2\sigma_3}{3} = \frac{q_c + 3\sigma_3}{3} \\ p_t = \frac{\sigma_3 + 2\sigma_1}{3} = \frac{-|q_t| + 3\sigma_1}{3} \end{cases}, \tag{3}$$

with the subscripts c and t for the compression and tension loading respectively.

The triaxial tests are used to characterize the shearing properties of the samples. The Mohr-Coulomb failure criterion expressed by Eq. 4 is used in this work to evaluate the shearing strength of the materials. It gives a linear relationship between the ultimate values (σ_N, $\tau_{\max}$). In the (p-q) plane, the criterion can be expressed as in Eq. 5. The advantage of the latter expression is that the failure criterion is directly obtained by a linear regression of (p,q_u) couples, while in the ($\sigma - \tau$) plane, the best tangent to the Mohr circles has to be evaluated [27].

$$\tau_{\max} = c + \sigma_N \tan \phi, \tag{4}$$

with $\tau_{\max}$, the ultimate shear stress, c the cohesion, σ_N the applied normal stress and ϕ the friction angle.

$$q_u = k + Mp, \tag{5}$$

with q_u the ultimate deviatoric stress, k the intercept, M the slope and p the mean stress.

As this work focuses on dry glass beads, the cohesion is negligible ($c \approx 0$ and $k \approx 0$). Therefore, the friction angle ϕ is characterizing the failure of the granular material. The M parameter is given in Eq. 6 for compression and tension testing.

$$M_c = \frac{q_{u,c}}{p_c} = \frac{6 \sin \phi_c}{3 - \sin \phi_c} \quad M_t = \frac{q_{u,t}}{p_t} = \frac{-6 \sin \phi_t}{3 + \sin \phi_t}, \tag{6}$$

with the subscripts c and t for the compression and tension loading respectively.

3.1 Triaxial compression

The membrane used for the triaxial compression tests is made of latex (with an elastic modulus $E = 1.11\,\text{MPa} \pm 0.03\,\text{MPa}$). This commercially available membrane with a thickness of 97 µm in average is used to encapsulate the granular

material into a tubular shape with a diameter $D \approx 36\,\text{mm}$. A two-part cylindrical mold is used to ensure the shape and dimensions of the sample, the granular material is poured in the membrane, the sample is sealed with O-rings and after vacuuming the sample (with a *VP4300* vacuum pump) to the desired confining pressure (thanks to the vacuum regulator), the sample is measured and placed under the loading frame for starting the loading procedure. The samples have a length $L = 78.73\,\text{mm} \pm 1.58\,\text{mm}$ and a diameter $D = 35.81\,\text{mm} \pm 0.50\,\text{mm}$. A 1 kN load cell (with a resolution of $\pm 0.5\%$ from 1% to 100% of the load cell value) has been used, as the compression forces measured during the validation tests were in this range.

The compression elastic modulus E_c is calculated from the initial slope of the stress-strain curve (in a linear region from 0% up to 0.4% of strain). The slope is calculated from the linear regression of the extracted region. The compression elastic modulus E_c is calculated on the last loading of the compression test. As the compression elastic modulus E_c is computed at low axial stress (and low strain), the mean stress p corresponds to the confining pressure ΔP. The ultimate stress $q_{u,c}$ is calculated as an average around the highest stress measured. Averaging over a small displacement region ($\pm 25\,\mu\text{m}$) allows for removing some noise in the measurement of the force and the peaks due to the stick-slip behavior of the failure.

3.2 Triaxial tension

The triaxial tensile testing is performed on cylindrical samples. Special caps have been designed and 3D printed to be hold by the grippers of the *LS1* universal testing machine. The membranes used for the tensile tests are made of natural rubber (latex, with an elastic modulus $E = 1.28\,\text{MPa} \pm 0.01\,\text{MPa}$ and a thickness of $363\,\mu\text{m}$ in average). Several diameters of samples have been tested and compared (with approximate diameters $D \approx 10 - 15 - 20\,\text{mm}$ and approximate lengths $L \approx 25 - 30 - 40\,\text{mm}$). The speed of the tests is constant and set at 5 mmmin. A 250N load cell (with a resolution of $\pm 0.5\%$ from 1% to 100% of the load cell value) has been used, as the tensile forces measured during the validation tests were in this range.

In order to remove the influence of the membrane, tensile tests with a confining pressure $\Delta P = 0\,\text{kPa}$ are performed. The three repetitions of these tests are averaged and removed from all the other tests with $\Delta P \geq 0\,\text{kPa}$ for removing the influence of the membrane and the deformation of the sample during the loading. The tension elastic modulus E_t is calculated from the initial slope of the stress-strain curve (in a linear region from 0% up to 0.4% of strain), similarly as for the compression tests.

3.3 Cantilever beam bending

The membrane used for these tests is the same as for the triaxial tension tests. The outputs of the bending tests are bending forces F_b and displacements δ_b that are converted into bending stresses and strains from Eq. 7 in order to remove the influence of the geometry and of the dimensions of the samples. It is important to note that the measured bending force is not taking the confinement into account (as in the case of compression and tensile tests). The deviatoric bending stress q_b corresponds to the pure bending stress due to the moment of force. The total axial stress σ_a is given by the sum of the deviatoric bending stress and the confining pressure (compression stress). In this work, only the pure bending stress is considered (the initial state being the confined state of the sample). Therefore, all the classical beam theory formulae can be applied to the deviatoric stress q_b. A 10 N load cell (with a resolution of $\pm 0.5\%$ from 1% to 100% of the load cell value) has been used, as the bending forces measured during the validation tests were in this range.

$$q_b = M_b \frac{y_{\max}}{I} = F_b \frac{4L}{\pi R^3} \quad \epsilon_b = \frac{q_b}{E_b} = \delta_b \frac{3R}{L^2}, \tag{7}$$

with M_b the bending moment, $y_{\max}$ the maximal distance between the neutral axis and an external fiber, I the second moment of area of the structure, E_b the equivalent bending

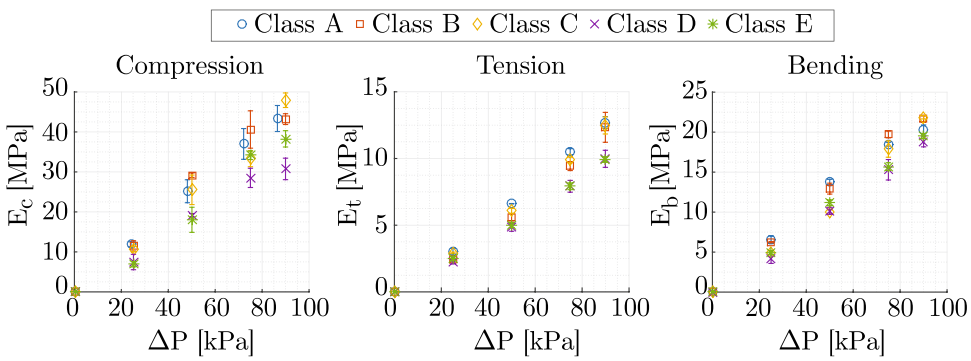

Fig. 4 Elastic moduli in compression, tension ($D \approx 15\,\text{mm}$) and bending for different glass beads and multiple confinements with a negligible impact of the class of the glass beads on the stiffness as the stiffness change is mainly due to the confining pressure

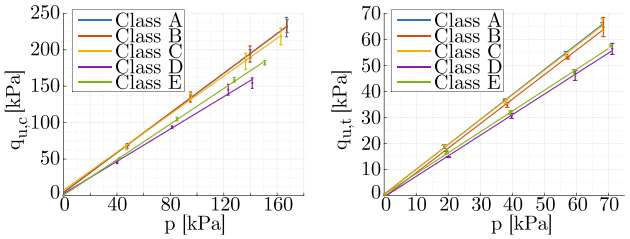

Fig. 5 Results of the ultimate deviatoric stresses in compression (left) and tension (right) for different glass beads and multiple pressure differences; for similar confinement, the compression strength is larger than the tension

elastic modulus, F_b the bending force, L the structure length (between the clamping and the point of application of the force) and δ_b the deflection of the structure where the force is measured.

A homogeneous and linear material following Hooke's law is assumed for the following relationships: $q_b = E_b \epsilon_b$ and $q_b = (M_b y_{\max})/I$. The bending stress is calculated at the point where the moment is maximum (critical point in the structure). For the cantilever bending, the moment of force is maximum at the clamping, giving $M_b = F_b L$.

The bending elastic modulus E_b is directly obtained from Eq. 8 from the experimental results at a given ΔP. It can also be calculated as the initial slope of the stress-strain curve between $\epsilon = 0\%$ and $\epsilon = 0.8\%$. The ultimate stress in bending $q_{u,b}$ corresponds to the maximum stress reached during a bending test.

$$E_b = \frac{\Delta F_b}{\Delta \delta_b} \frac{L^3}{3I} = \frac{\Delta F_b}{\Delta \delta_b} \frac{4L^3}{3\pi R^4} \tag{8}$$

4 Experimental results

The influence of the confining pressure on the elastic moduli in compression, tension and bending is shown in Fig. 4. The influence of the grain size is negligible with respect to the confining pressure, while for increased ΔP, the moduli are increasing. The pressure difference ΔP is the main factor driving the elastic properties. A linear evolution can be assumed for the range of pressures studied in this work (between $\Delta P = 0$ kPa and $\Delta P = 90$ kPa), as expressed in Eqs. 9 to 11.

$$E_c[\text{MPa}] = 9.68 - 0.01\bar{d}[\mu\text{m}] + 0.59\Delta P[\text{kPa}], \tag{9}$$

$$E_t[\text{MPa}] = 0.50 - 0.001\bar{d}[\mu\text{m}] + 0.12\Delta P[\text{kPa}], \tag{10}$$

$$E_b[\text{MPa}] = 1.06 - 0.003\bar{d}[\mu\text{m}] + 0.23\Delta P[\text{kPa}], \tag{11}$$

with $\bar{d}$ the mean diameter of the glass beads.

Figure 5 shows the influence of the confining pressure on the ultimate compression deviatoric stress $q_{u,c}$. Presenting the ultimate deviatoric stress $q_{u,c}$ as a function of the mean stress p is suitable to represent the Mohr-Coulomb failure criterion. The slope of the linear regression through the ultimate deviatoric stresses can be translated into friction angle ϕ and the intercept can give the cohesion c of the material. As expected, the cohesion is very low ($c = 2.21$ kPa $\pm$ 1.75 kPa, negligible with respect to the measured stresses) as the granular materials are dry glass beads embedded in a latex membrane. The averaged friction angle from the Mohr-Coulomb criterion for the different glass beads is $\phi_c = 32.3° \pm 2.7°$. The calculation of the friction angle is performed through a linear regression over the experimental data. For this regression, the cohesion c is forced to be null (with $q = Mp$ as fitting model).

By drawing the ultimate deviatoric stress $q_{u,t}$ as a function of the mean stress p (Fig. 5), the Mohr-Coulomb failure criterion can be easily obtained by a linear regression. The size of the grains has a very low influence on the failure of the sample. In theory, the cohesion c of dry granular material should be null. The values obtained from the tensile tests are negligible compared to the measured stresses, confirming that without a confinement, the granular material cannot resist any force. The average of friction angles for a sample with $D = 14.56$ mm is $\phi_t = 31.6° \pm 4.1°$ which is very similar to the compression results. The calculation of the friction angle is performed through a linear regression with a null cohesion over the experimental data.

The linear model given in Eq. 12 for the compression strength has been obtained experimentally and verified by ANOVA method. This model shows that the larger the glass beads, slightly lower will be the compression strength, while if the confining pressure is increased, the strength is greatly increased.

$$q_{u,c}[\text{kPa}] = 49.48 - 0.05\bar{d}[\mu\text{m}] + 2.66\Delta P[\text{kPa}] \tag{12}$$

The tension strength is also following a linear relationship with the mean stress p or the confining pressure ΔP. The

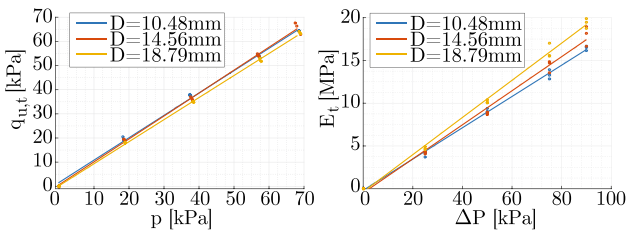

Fig. 6 Comparison of the tensile strength (left) and the tensile elastic modulus (right) for different diameters of samples (examples illustrated with the class C glass beads)

linear model given in Eq. 13 has been obtained experimentally and verified by ANOVA method. As for the compression, lower sizes of glass beads lead to larger strength of the sample while large pressure differences lead to an increase in tensile strength.

$$q_{u,t}[\text{kPa}] = 2.81 - 0.006\bar{d}[\mu\text{m}] + 0.68\Delta P[\text{kPa}] \quad (13)$$

The diameter of the sample has very low influence on the mechanical properties of the granular jamming. Figure 6, shows on the left, the Mohr-Coulomb failure criterion in the (p-q) plane and on the right, the evolution of the tension elastic modulus E_t with respect to the confining pressure ΔP for glass beads of the class C. The tension elastic modulus E_t seems to be slightly larger at higher confining pressures and diameters but follows similar relationships. The calculated friction angle ϕ_t (mean variation of 3.7% and maximum variation of 7.4%) and cohesion parameter c (mean variation of 0.67 kPa and maximum variation of 0.88 kPa) are very similar for the different diameters of the samples. The diameter of the sample has low influence on the mechanical properties (elastic characteristics and strength) of the structure.

5 Modeling

Most of the current works perform separated characterizations either by compression of the granular material [7, 12, 20], by bending of a beam [7, 15, 17, 18, 28] or by a characterization of the membrane in tension [29, 30]. A model linking the granular material compression and a robotic arm bending behavior has been initiated in [31] but only the ultimate state could be estimated. Most of the bending models rely on finite or discrete elements modeling and not analytical models [5, 22]. In this work, the analytical models are proposed for simplified modeling of the granular jamming towards various mechanical applications. The granular material is modeled as a homogeneous material following Hooke's law. Furthermore, an elastic perfectly plastic representation is used. The elastic model is developed for the reversible deformation at small strain (for which the experimental results are linear and reversible).

5.1 Compression-tension model

As seen previously, the friction angles in tension and compression can be assumed to be equal to each other ($\phi_c = \phi_t = \phi$). An experimental linear relationship between the axial stress σ_a and the radial stress σ_r has been proven in this work and in [32]. Therefore, it is possible to combine the compression and tension strengths for a given pressure difference ΔP (Eq. 14, obtained from Eqs. 3, 5 and 6) or for a given mean pressure p (Eq. 15, obtained from Eqs. 5 and 6). These equations only depend on the material's characteristics (the friction angle ϕ). The strength in compression will always be larger than the strength in tension (in absolute value) because $\frac{1-\sin(\phi)}{1+\sin(\phi)} \leq 1$ for $\phi = 0°$ to $90°$.

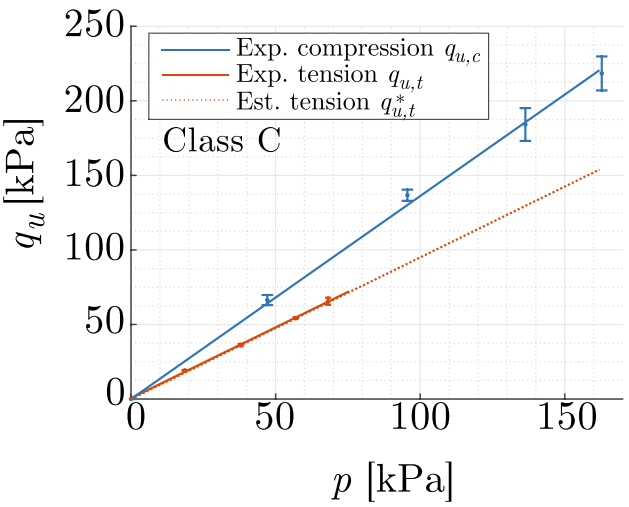

Fig. 7 Tension estimation ($q^*_{u,t}$) from the compression experimental results ($q_{u,c}$), compared to the experimental tension results ($q_{u,t}$)

$$q_{u,t}|_{\Delta P} = -\, q_{u,c}|_{\Delta P} \frac{1-\sin\phi}{1+\sin\phi} \quad (14)$$

$$q_{u,t}|_{p} = -\, q_{u,c}|_{p} \frac{3-\sin\phi}{3+\sin\phi} \quad (15)$$

It is then possible to estimate the tension ultimate strength $q_{u,t}$ from the friction angle ϕ and the compression ultimate strength $q_{u,c}$. This correspondence is useful to simplify the experimental characterization of a granular material. Indeed, as the tension behavior can be deduced from the outputs of the compression characterization, tension tests are no longer to be performed. The comparison between the estimated value and the experimental measurement is illustrated in Fig. 7 for a given class of glass bead (class C) to simplify the representation. Knowing the friction properties of the granular material in compression ϕ_c and its strength $q_{u,c}$ is sufficient to characterize the failure in tension. As the experiments are giving a slight difference in the value of the friction angle in compression and in tension, the model is however not perfectly fitting the experimental results and a negligible absolute error is measured. Notice that a difference of 1° on the friction angle leads to an error smaller than 4% on the estimation of $q_{u,t}$, which is acceptable. A linear regression crossing the origin of the axes ($q = Mp$) is used.

Another possibility to compare the compression and tension strengths is to find the corresponding pressure difference to both situations (in compression and in tension).

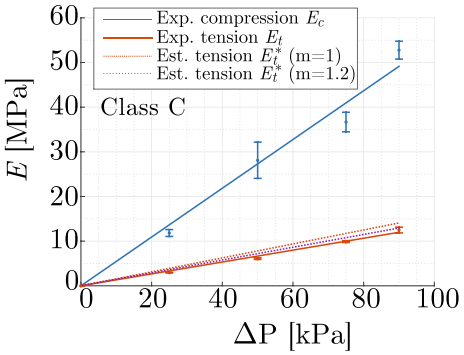

Fig. 8 The strength can be accurately estimated and the exponential model with $m = 1.2$ gives satisfying results for the elastic modulus estimation, while the linear model with $m = 1$ is giving slightly different results

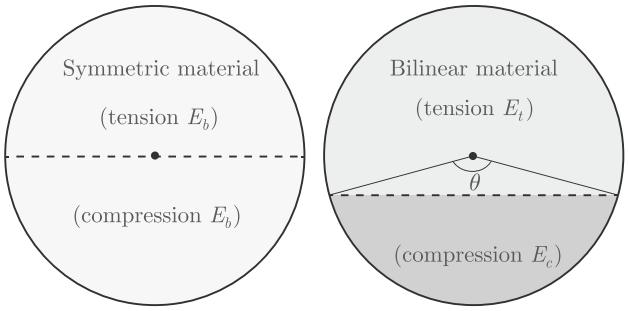

Fig. 9 Single material representation (left), with symmetric elastic properties (E_b) and the neutral axis (dashed line) passing through the centroid of the disk; single bilinear material representation (right), with asymmetric elastic properties (E_t in tension, E_c in compression) where the neutral axis (the chord defined by the θ angle) delimits a smaller region for the compression due to its higher elastic modulus ($E_c > E_t$)

Indeed, for a given pressure difference ΔP, the strength obtained in tension will correspond to the strength in compression at a different pressure difference ΔP_{eq}. In order to find this relationship, the equivalent ultimate strengths in tension and compression can be linked. It is possible to find the equivalent confining pressure ΔP_{eq} at which the compression strength corresponds to the tensile strength at ΔP ($q_{u,c}|_{\Delta P_{\text{eq}}} = \left| q_{u,t}|_{\Delta P} \right|$). The equivalent confining pressure ΔP_{eq} is given in Eq. 16. Notice that $\Delta P_{\text{eq}} \leq \Delta P$.

$$\Delta P_{\text{eq}} = \frac{1 - \sin(\phi)}{1 + \sin(\phi)} \Delta P \tag{16}$$

The link between the compression and the tension strengths has been highlighted. These tests are similar but the applied tension axial stress is actually decreasing the confinement applied on the sample. As the triaxial compression and tension tests show similar failure results for a given working condition (effective confining pressure), it can be assumed that the elastic behavior is also similar. Indeed, a confining pressure ΔP fully characterizes the strength and elastic properties of a specific granular material, which means that for a given working condition, the elastic modulus and strength are set.

Using the equivalent confining pressure to verify the correspondence between the compression and the tension tests leads to Fig. 8. The theory has been developed based on the failure of the samples (and the estimated strength in tension is very close to the experimental results), but it is assumed that the correspondence can be extended to the elastic moduli. Indeed, a working point corresponds to a specific situation in which the tension and compression strengths are similar. It is therefore possible to estimate the tensile elastic modulus E_t from the compression elastic modulus E_c, using the relationship between the confining pressure ΔP and the equivalent confining pressure ΔP_{eq}.

Assuming that the compression modulus is following an exponential law such as $E_c|_{\Delta P} = a(\Delta P)^m$ [26], the tension modulus can be obtained by Eq. 17. Fitting the compression experimental results on this exponential model leads to $n = 1.2$ for class C glass beads. The linear model leads to $n = 1$, and gives results slightly less close to the experimental data.

$$E_t^*|_{\Delta P} = E_c|_{\Delta P_{\text{eq}}} = \left(\frac{1 - \sin(\phi)}{1 + \sin(\phi)} \right)^m E_c|_{\Delta P}, \tag{17}$$

with E_t^* the estimated tension elastic modulus.

5.2 Bending model

As the granular jamming structures are not always subjected to axial loads, but also to bending in various applications, a bending model is proposed. The granular jamming can be modeled from two different representations (Fig. 9) as introduced in [31]. The first corresponds to a single homogeneous symmetric material (with an equivalent bending modulus E_b) and is compared to a second representation of a single homogeneous bilinear material (with a modulus E_t in tension and a modulus E_c in compression). The neutral axis separates the part in tension and the part in compression (its position is obtained from the equilibrium in internal axial forces N developed in Eq. 18).

$$N = \int_A \sigma dA = 0 \tag{18}$$

The solution is assumed to present an initial elastic phase (linear region in the stress-strain curve) and a plastic zone (giving permanent deformation, due to grains reorganization). Only the elastic model is developed in this work, as the goal of this work is to evaluate the stiffness under

confinement, therefore at low strain levels and under elastic deformation.

In compression, it is assumed that the sample withstands only compression stress due to the external confinement and due to the axial loading. In tension, it is assumed that the sample withstands a decreased compression stress due to the axial loading opposed to the confining pressure. In bending, a simple bending condition is assumed after a compression stress is applied due to the confinement. During the bending, a part of the sample will undergo tension and the other part compression [33].

It is important to note that the experimental compression, tensile and bending tests are giving deviatoric stresses q. Therefore, the ultimate stress corresponds to the ultimate deviatoric strength q_u. It is considered that the initial state corresponds to the confined state (after applying the confining pressure ΔP) for all the mechanical tests. Therefore, the compression, tension and bending stresses are deviatoric stresses.

A cylindrical sample with a radius R is considered in this study. In order to characterize the geometry of the asymmetric structure, the disk is divided in two circular segments defined by the angle θ, making a chord corresponding to the neutral axis (Fig. 9). The areas of the two sectors are given by Eqs. 19 and 20.

$$A_t = \frac{R^2}{2}\left(2\pi - \theta + \sin\theta\right), \tag{19}$$

$$A_c = \frac{R^2}{2}\left(\theta - \sin\theta\right), \tag{20}$$

where subscripts t and c indicate the sections in tension and in compression respectively (corresponding to the smallest and the biggest sections in this description of the problem).

The centroids of these sections, with respect to the neutral axis, are given in Eqs. 21 and 22. The position of the neutral axis y_{na} with respect to the center of the disk is given in Eq. 23.

$$\tilde{y}_t^* = \frac{4}{3}\frac{R(\sin(\theta/2))^3}{2\pi - \theta + \sin\theta} + R\cos(\theta/2) \tag{21}$$

$$\tilde{y}_c^* = -\frac{4}{3}\frac{R(\sin(\theta/2))^3}{\theta - \sin\theta} + R\cos(\theta/2) \tag{22}$$

$$y_{na} = -R\cos(\theta/2) \tag{23}$$

The second moment of area of the disk I_b, calculated at the centroid of the disk, is expressed in Eq. 24. The parallel axis theorem is used to compute the second moment of area at a distance y_{na}. The second moments of area for the two circular segments (in compression I_c^* and in tension I_t^*) are calculated with respect to the neutral axis and are expressed in Eqs. 25 and 26.

$$I_b = \frac{\pi R^4}{4} \tag{24}$$

$$I_c^* = \frac{R^4}{24}\left(9\theta - 14\sin\theta - \cos\theta\sin\theta + 6\theta\cos\theta\right) \tag{25}$$

$$I_t^* = \frac{\pi R^4}{4}\left(3 + 2\cos\theta\right) - I_c^* \tag{26}$$

The two representations of the structure should be equivalent in terms of mechanical behavior. Therefore, a relationship between E_b, for the single symmetric material, and (E_c, E_t) for the asymmetric structure is developed for the elastic moduli in the elastic region.

As pure bending is considered, no normal stress acts on the structure (as the initial condition is set after the confinement which is constant). Therefore, the neutral axis position can be found by the equilibrium of normal forces N expressed in Eq. 27 [34].

$$N = \int_{A_t}\sigma_t dA + \int_{A_c}\sigma_c dA = -\frac{E_t S_t + E_c S_c}{\rho} = 0, \tag{27}$$

with S_t and S_c the first moment of area of the part respectively in tension and in compression and ρ the radius of curvature.

Due to the condition on the neutral axis (being the reference axis in this elastic model), the part with the highest value of elastic modulus will have the smallest area in order to respect the equilibrium condition (as seen in Eq. 28). From the experiments, it has been observed that the compression elastic modulus E_c is higher than the tension one E_t, therefore the compression part will be smaller than the tension part.

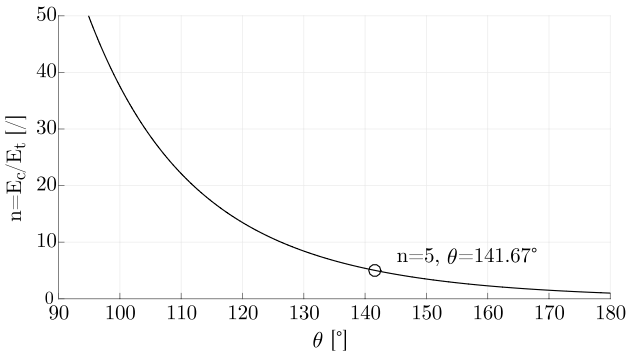

Fig. 10 Evolution of the elastic moduli ratio n with respect to the angle θ in a bilinear disk, illustrated by an example for a ratio of $n = E_c/E_t = 5$ giving $\theta = 141.67°$

$$E_t S_t + E_c S_c = E_t \widetilde{y}_t^* A_t + E_c \widetilde{y}_c^* A_c = 0, \tag{28}$$

with $\widetilde{y}^*$, E, A being respectively the position of the centroid with respect to the neutral axis, the elastic modulus and the area of the section, with the subscripts t for tension and c for compression.

As the neutral axis is the reference axis ($y_{na}^* = 0$), the ratio of elastic moduli in compression and tension is linked to the positions of the centroids (Eq. 29). There is no analytical solution for writing the angle θ as a function of the elastic moduli ratio n (combining Eq. 29 with Eqs. 21 and 22). Therefore, the equation is solved numerically and illustrated in Fig. 10. Depending on the ratio of elastic moduli n, the angle characterizing the geometry of the bilinear structure can be easily defined. For instance, an elastic moduli ratio of $n = 5$ gives an angle of $\theta = 141.67°$.

$$n = \frac{E_c}{E_t} = -\frac{\widetilde{y}_t^* A_t}{\widetilde{y}_c^* A_c} \tag{29}$$

Finally, in a bilinear structure the curvature ψ is given by Eq. 30 [34]. Therefore, the equivalent bending modulus E_b will be given by Eq. 31. As it can be seen, the different second moments of area I_t^*, I_c^* and I_b are proportional to R^4. Therefore, the equivalent bending modulus E_b is independent of R and, then, of the dimensions of the structure.

$$\psi = \frac{1}{\rho} = \frac{M_b}{E_t I_t^* + E_c I_c^*} = \frac{M_b}{E_b I_b}, \tag{30}$$

with ψ the curvature, ρ being the radius of curvature and E_b the equivalent bending elastic modulus.

$$E_b = \frac{E_t I_t^* + E_c I_c^*}{I_b}, \tag{31}$$

with I and E the second moment of area of a section and its corresponding elastic modulus, with subscripts b, t, c for the section respectively in bending, in tension and in compression.

Figure 11 gives the results for the analytical model computing E_b as a function of E_c and E_t as expressed in Eq. 31. The residuals of this model are illustrated for the different confining pressures ΔP and for the different classes of glass beads. As it can be seen, the model predicts in a very satisfying manner the equivalent elastic modulus in bending from the compression and tensile characterization. Linear regressions of the evolution of the moduli with respect to the pressure difference ΔP are used in the model to have a continuous evaluation. The model for class A to C gives slightly over-estimated values while the model for class D and E gives slightly under-estimated values. The relative error on the linear regression is constant and lower than 10% for all the glass beads while the absolute error is slightly increasing with the pressure difference ΔP. This relative error corresponds actually to the relative error on the slopes of the linear regressions ($|(E_b - E_b^*)/E_b| = |(\kappa \Delta P - \kappa^* \Delta P)/(\kappa \Delta P)| = |(\kappa - \kappa^*)/\kappa|$ with κ the slope of the linear regression and * indicating the estimation). When the experimental points are compared with the model, the lower pressure differences give lower satisfaction (with a relative error close to 20%). At low ΔP, the elastic modulus is low and therefore a small error on its estimation impacts strongly the relative error. The linear regression estimation is very satisfying.

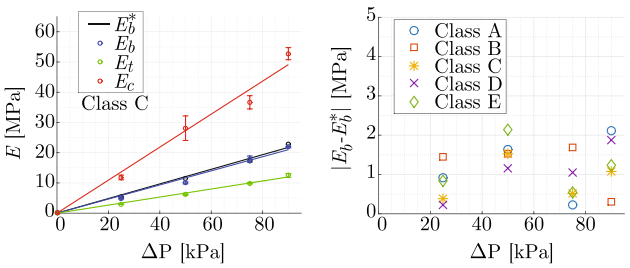

Fig. 11 The estimation of the bending elastic modulus can be obtained from a combination of the compression and tension modulus (E_c and E_t) and is compared to the experimental results (the model gives a proper correspondence between the estimate E_b^* and the experimental data E_b)

5.3 Considering the membrane

In the previous models, only the granular material has been studied. As the granular material has to be encapsulated in a membrane in order to set the pressure difference, the effect of the membrane has to be taken into account for possible applications.

Assuming an elastic deformation, with small strains, the flexural rigidity of the solution EI_{tot} is given by the sum of the flexural rigidity of the granular material EI_{gran} and the one of the membrane EI_{mem} (Eq. 32).

$$EI_{\text{tot}} = EI_{\text{gran}} + EI_{\text{mem}} \tag{32}$$

The membrane can be seen as a hollow cylinder with a thickness t and an inner diameter D_{in}. The corresponding outer diameter is $D_{\text{out}} = D_{\text{in}} + 2t$. Therefore, the granular material corresponds to a solid cylinder with a diameter $D = D_{\text{in}}$.

The experimental tension elastic modulus with a confinement $\Delta P = 0\,\text{kPa}$ gives $E_0 \approx 279\,\text{kPa}$ for a sample of diameter $D = 14.56\,\text{mm}$ (averaged for the different sizes of glass beads). Calculating the flexural stiffness of the sample (granular material and membrane) leads to $E_0 I_0 = 615\text{Nmm}^2$, while the flexural stiffness of the membrane alone ($E_{\text{mem}} = 1.28\,\text{MPa}$ for the latex

membrane) with $D_{in} = 14.56\,\text{mm}$ and $D_{out} = 15.29\,\text{mm}$ gives $E_{mem}I_{mem} = 610\,\text{Nmm}^2$. Therefore, the granular jamming with no confinement has a negligible impact of the apparent stiffness of the solution. In the condition of no confinement, the elasticity of the structure is actually governed by the membrane. The bending experiments confirm this model (the elasticity of the structure is due to the membrane when the confinement is $\Delta P = 0\,\text{kPa}$).

The performance of the granular jamming solution can be evaluated based on the absolute flexural rigidities that can be achieved and the stiffness change $\alpha = EI_{rig}/EI_{flex}$. As the flexural rigidities depend on the dimensions of the structure, a comparison based on the corresponding equivalent elastic modulus E is proposed. Assuming a circular cross-section, with a membrane (hollow circular section of dimensions D_{in} and $D_{out} = D_{in} + 2t$) surrounding the granular material, the rigid state ($\Delta P > 0\,\text{kPa}$) is given by the contribution of the membrane (subscript 'mem') and of the granular material (subscript 'gran') while the flexible state ($\Delta P = 0\,\text{kPa}$) is given by the contribution of the membrane only. The stiffness gain is therefore given in Eq. 33.

$$\begin{aligned}\alpha = \frac{EI_{rig}}{EI_{flex}} &= \frac{E_{mem}I_{mem} + E_{gran}I_{gran}}{E_{mem}I_{mem}} \\ &= 1 + \frac{E_{gran}}{E_{mem}}\frac{D_{in}^4}{D_{out}^4 - D_{in}^4} \\ &= 1 + \frac{E_{gran}}{E_{mem}}\frac{1}{\left(\frac{D_{out}}{D_{in}}\right)^4 - 1}\end{aligned} \tag{33}$$

In general, the thickness of the membrane is much smaller than the inner diameter ($t \ll D_{in}$), giving therefore Eq. 34.

$$\alpha \approx 1 + \frac{E_{gran}}{E_{mem}}\frac{D_{in}}{8t} \tag{34}$$

Knowing the elastic moduli of the different membranes and their dimensions, as well as the granular jamming properties of the glass beads, it is possible to calculate the resulting elastic moduli in the rigid and flexible states of the granular jamming-based structures developed in this work (illustrated in Fig. 12). These structures are compared to solutions proposed in the literature. The performance of the proposed structures is promising. The granular jamming based on parylene and HDPE membranes ($E_{parylene} = 2856\,\text{MPa}$ [35], $E_{HDPE} = 608\,\text{MPa} \pm 21\,\text{MPa}$) are projections calculated from Eq. 33 (based on the results of class A beads with $E_b|_{90\,\text{kPa}} = 20.26\,\text{MPa}$, because of the limited diameter of the membranes). The granular jamming based on latex membranes is given for class C glass beads giving the best results in terms of elastic modulus in the rigid state ($\Delta P = 90\,\text{kPa}$ and $E_b|_{90\,\text{kPa}} = 21.86\,\text{MPa}$).

As it can be seen in Fig. 12, the range of elastic moduli reached in this work is similar to the one given in the literature but miniaturized solutions are proposed and compared to the current state of the art. The effect of the membrane is strongly impacting the flexible state of the solutions for decreasing diameters. The small-dimension membranes are made of thinner but stiffer materials than the latex used for larger samples. Therefore, a limitation towards miniaturization could be the stiffness of the membrane causing a limited flexible state at low pressure differences. The stiffness change due to the granular material is hidden by the fixed and large stiffness of the membrane and the global stiffness gain α is low.

For similar membranes (e.g. latex membranes with a given thickness), when the diameter decreases, the rigid state is slightly decreasing and the flexible state increases further. This is due to the fact that the membrane impacts more and more the global stiffness as its thickness has a larger impact on the second moment of area I compared to the granular material elastic modulus E. It is important to note that for larger diameters ($D \geq 15\,\text{mm}$), the rigid state of the latex, HDPE and parylene membranes samples are similar but the flexible state is much softer for the latex membrane samples, offering therefore a larger stiffness gain α. The applications

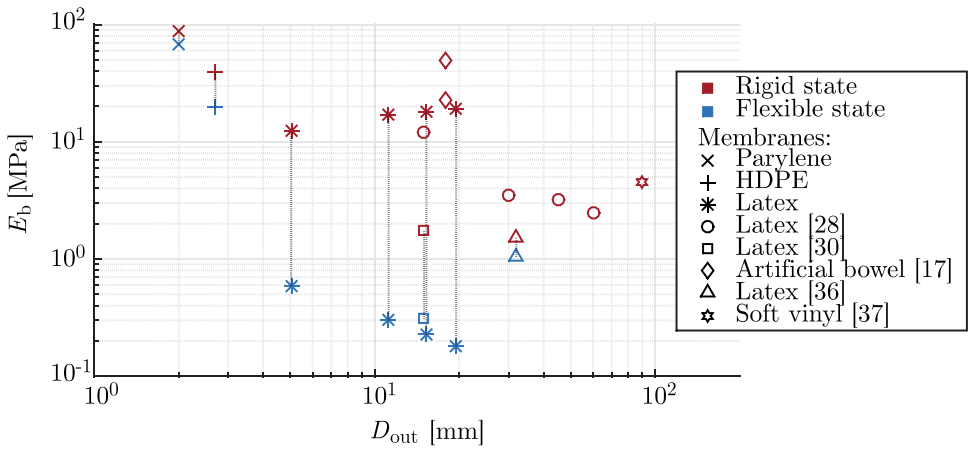

Fig. 12 Performance of the granular jamming solutions in terms of equivalent elastic modulus in bending E_b with respect to the outer diameter D_{out} of the cylindrical structure. The upper marker corresponds to the rigid state and the lower marker (if existing) corresponds to the flexible state. The results of this work are presented for the parylene ($D_{out} = 2.0\,\text{mm}$), HDPE ($D_{out} = 2.7\,\text{mm}$) and latex ($D_{out} = 5.03 \rightarrow 19.51\,\text{mm}$) membranes

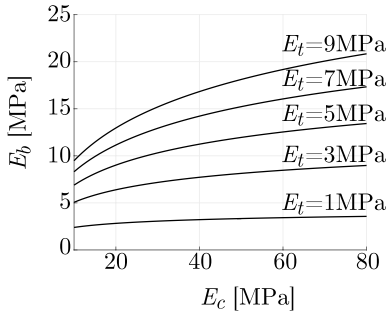

Fig. 13 Sensitivity analysis of the analytical model. The tension elastic modulus E_t has a larger influence on the value of E_b than the compression elastic modulus E_c

that can be targeted with miniaturized granular jamming structures are therefore also limited due to the small stiffness gain.

5.4 Sensitivity analysis

A sensitivity analysis of the analytical model is illustrated in Fig. 13. The tension elastic modulus E_t is influencing more the bending modulus E_b than the compression modulus E_c. This means that a small error on the tension modulus E_t will have a larger impact on the estimation of the bending modulus E_b than an error on the compression modulus E_c. For low values of tension elastic modulus E_t, the bending elastic modulus E_b is almost not impacted by a change in compression modulus E_c.

6 Conclusion

The granular jamming mechanism has been characterized under different loading conditions as a solution for tunable stiffness structures. The stiffness change has been evaluated thanks to the measurement of the elastic moduli obtained for different glass beads at various pressure differences. The stiffness and strength are the largest in compression and the smallest in tension. The size of the particles has a low impact on the stiffness while the stiffness is increasing almost linearly with the pressure difference. A linear relationship between the pressure difference and the strength of the sample has been observed and confirmed from the theory. A null cohesion has been confirmed as it is negligible in dry granular materials. The stiffness in compression can be estimated as evolving linearly with respect to the confinement, in the range of studied pressure differences. Nevertheless, an exponential model can also be used.

The analytical model of the granular jamming presented in this work is a useful tool for predicting the bending behavior of structures based on granular jamming. This development is an important result that can help saving time for designing mechanical structures based on the granular jamming principle. Knowing the granular material characteristics (friction angle ϕ) and knowing the compression elastic modulus E_c, the tension elastic modulus E_t can be deduced from the compression elastic modulus E_c with no need of additional mechanical tests. The proposed model gives the relationship between E_t and E_c with respect to the mean pressure p or the pressure difference ΔP. The triaxial compression of granular material is very well known and routinely performed in geomechanics, which means that data may be directly available in the literature or easily obtained.

Finally, the bending elastic modulus E_b can be obtained from the two previous moduli E_c and E_t and the geometric consideration of the problem. Knowing the ratio of compression and tension elastic moduli n, the geometry of the equivalent asymmetric material beam can be determined. From this geometric consideration, the equivalent bending modulus E_b can be estimated. The model is giving very promising results and fits properly the experimental results.

These models can be used to estimate the stiffness performance of a structure based on granular jamming under different loading conditions. If the compression characteristics are known, the friction angle of the granular material can be calculated. The tension characteristics can be deduced from the previous experimental values and finally, the bending behavior can be estimated from these results. The models developed in this work target general mechanical applications for which the structure will mainly encounter bending. Designing granular jamming solutions requires, therefore, less experimental work thanks to the models proposed in this work.

Acknowledgements This work was supported by the Fonds de la Recherche Scientifique (FRS-FNRS) through an F.R.I.A. (Fonds pour la Formation à la Recherche dans l'Industrie et dans l'Agriculture) grant, a C.D.R (Crédit de Recherche) J.0098.19 and a Research Project P.D.R. (Projet de Recherche) T1002.14. L. Blanc would like to thank the Fonds David et Alice Van Buuren and the Fondation Jaumotte-Demoulin.

Author Contributions All authors contributed to the study conception and design. Material preparation, data collection and analysis were performed by Loïc Blanc, with the help and under the supervision of Bertrand François, Alain Delchambre and Pierre Lambert. The first draft of the manuscript was written by Loïc Blanc and all authors commented on previous versions of the manuscript. All authors read and approved the final manuscript.

Availability of data and material The datasets generated during and analyzed during the current study are available from the corresponding author on reasonable request.

Compliance with ethical standards

Conflict of interest The authors declare that they have no conflict of interest.

References

1. Loeve, A., Breedveld, P., Dankelman, J.: Scopes too flexible... and too stiff. IEEE Pulse **1**(3), 26 (2010)
2. Blanc, L., Delchambre, A., Lambert, P.: Flexible medical devices: review of controllable stiffness solutions. In: Actuators, vol. 6, p. 23. Multidisciplinary Digital Publishing Institute (2017)
3. Cianchetti, M., Laschi, C., Menciassi, A., Dario, P.: Biomedical applications of soft robotics. Nat. Rev. Mater. **3**, 1 (2018)
4. Kuder, I.K., Arrieta, A.F., Raither, W.E., Ermanni, P.: Variable stiffness material and structural concepts for morphing applications. Prog. Aerosp. Sci. **63**, 33 (2013)
5. Brigido-González, J.D., Burrow, S.G., Woods, B.K.: Switchable stiffness morphing aerostructures based on granular jamming. J. Intell. Mater. Syst. Struct. **30**(17), 2581 (2019)
6. Bajkowski, J.M., Dyniewicz, B., Bajer, C.I.: Damping properties of a beam with vacuum-packed granular damper. J. Sound Vib. **341**, 74 (2015)
7. Cheng, N.G., Lobovsky, M.B., Keating, S.J., Setapen, A.M., Gero, K.I., Hosoi, A.E., Iagnemma, K.D.: Design and analysis of a robust, low-cost, highly articulated manipulator enabled by jamming of granular media, In: IEEE International Conference on Robotics and Automation (ICRA) (IEEE), pp. 4328–4333 (2012)
8. Mustaza, S.M., Mahdi, D., Saaj, C., Albukhanajer, W.A., Lekakou, C., Elsayed, Y., Fras, J.: Tuneable stiffness design of soft continuum manipulator. In: International Conference on Intelligent Robotics and Applications, pp. 152–163. Springer, New York (2015)
9. Langer, M., Amanov, E., Burgner-Kahrs, J.: Stiffening sheaths for continuum robots. Soft Robot. **5**(3), 291 (2018)
10. Manti, M., Cacucciolo, V., Cianchetti, M.: Stiffening in soft robotics: a review of the state of the art. IEEE Robot. Autom. Mag. **23**(3), 93 (2016)
11. Jaeger, H.M.: Celebrating soft matter's 10th anniversary: toward jamming by design. Soft Matter **11**(1), 12 (2015)
12. Brown, E., Rodenberg, N., Amend, J., Mozeika, A., Steltz, E., Zakin, M.R., Lipson, H., Jaeger, H.M.: Universal robotic gripper based on the jamming of granular material. Proc. Natl. Acad. Sci. **107**(44), 18809 (2010)
13. Amend, J.R., Brown, E., Rodenberg, N., Jaeger, H.M., Lipson, H.: A positive pressure universal gripper based on the jamming of granular material. IEEE Trans. Robot. **28**(2), 341 (2012)
14. Amend, J., Cheng, N., Fakhouri, S., Culley, B.: Soft robotics commercialization: jamming grippers from research to product. Soft Robot. **3**(4), 213 (2016)
15. Wei, Y., Chen, Y., Ren, T., Chen, Q., Yan, C., Yang, Y., Li, Y., Novel, A.: Variable stiffness robotic gripper based on integrated soft actuating and particle jamming. Soft Robot. **3**(3), 134 (2016)
16. De Falco, I., Cianchetti, M., Menciassi, A.: STIFF-FLOP surgical manipulator: design and preliminary motion evaluation. In: Proceedings of 4th WorkShop on Computer/Robot Assisted Surgery (CRAS), pp. 131–134 (2014)
17. Loeve, A.J., van de Ven, O.S., Vogel, J.G., Breedveld, P., Dankelman, J.: Vacuum packed particles as flexible endoscope guides with controllable rigidity. Granul. Matter **12**(6), 543 (2010)
18. Cianchetti, M., Ranzani, T., Gerboni, G., De Falco, I., Laschi, C., Menciassi, A.: STIFF-FLOP Surgical manipulator: mechanical design and experimental characterization of the single module. In: IEEE/RSJ International Conference on Intelligent Robots and Systems (IROS) (IEEE), pp. 3576–3581 (2013)
19. Jiang, A., Adejokun S., Faragasso, A., Althoefer, K., Nanayakkara, T., Dasgupta, P.: The granular jamming integrated actuator. In: IEEE International Conference on Advanced Robotics and Intelligent Systems (ARIS) (IEEE), pp. 12–17 (2014)
20. Athanassiadis, A.G., Miskin, M.Z., Kaplan, P., Rodenberg, N., Lee, S.H., Merritt, J., Brown, E., Amend, J., Lipson, H., Jaeger, H.M.: Particle shape effects on the stress response of granular packings. Soft Matter **10**(1), 48 (2014)
21. Bardet, J.P.: Experimental Soil Mechanics, Experimental Soil Mechanics. Prentice Hall, New Jersey (1997)
22. Huijben, F.A.A.: Vacuumatics: 3D formwork systems. Ph.D. thesis, University of Eindhoven (2014)
23. Blanc, L., Pol, A., François, B., Delchambre, A., Lambert, P., Gabrieli, F.: Granular jamming as controllable stiffness mechanism for medical devices. In: Micro to MACRO Mathematical Modelling in Soil Mechanics, pp. 57–66. Springer, New York (2018)
24. Güneyli, H., Rüşen, T.: Effect of length-to-diameter ratio on the unconfined compressive strength of cohesive soil specimens. Bull. Eng. Geol. Environ. **75**(2), 793 (2016)
25. Nova, R., Wood, D.M.: A constitutive model for sand in triaxial compression. Int. J. Numer. Anal. Methods Geomech. **3**(3), 255 (1979)
26. Hicher, P.Y.: Elastic properties of soils. J. Geotech. Eng. **122**(8), 641 (1996)
27. Nova, R., et al.: Nova, roberto and others. In: Soil Mechanics (Wiley Online Library), chap. 5, pp. 125–239 (2010)
28. Yanagida, T., Adachi, K., Nakamura, T.: Development of endoscopic device to veer out a latex tube with jamming by granular materials. In: Proceedings of the 2013 IEEE International Conference on Robotics and Biomimetics (ROBIO) (IEEE), pp. 1474–1479 (2013)
29. Huijben, F., Herwijnen, F.V., Nijsse, V.R.: Acuumatics; systematic flexural rigidity analysis. In: Proceedings of the International Association for Shell and Spatial Structures (IASS) Symposium , pp. 8–12 (2010)
30. Jiang, A., Ranzani, T., Gerboni, G., Lekstutyte, L., Althoefer, K., Dasgupta, P., Nanayakkara, T.: Robotic granular jamming: does the membrane matter? Soft Robot. **1**(3), 192 (2014)
31. Cheng, N.G.: Design and analysis of jammable granular systems. Ph.D. thesis, Massachusetts Institute of Technology (2013)
32. Corfdir, A., Sulem, J.: Comparison of extension and compression triaxial tests for dense sand and sandstone. Acta Geotech. **3**(3), 241 (2008)
33. Jones, R.M.: Stress-strain relations for materials with different moduli in tension and compression. AIAA J. **15**(1), 16 (1977)
34. Frey, F.: Analyse des structures et milieux continus: mécanique des structures. PPUR presses polytechniques (2014)
35. Kang, D., Standley, A., Chang, J.H.C., Liu, Y., Tai, Y.C.: Effects of deposition temperature on Parylene-C properties. In: Proceedings of the 2013 IEEE 26th International Conference on Micro Electro Mechanical Systems (MEMS) (IEEE), pp. 389–390 (2013)